

Development of lithium hydroxide-metal organic framework-derived porous carbon composite materials for efficient low temperature thermal energy storage

Xiangyu Yang ^{a,c}, Shijie Li ^b, Jianguo Zhao ^{a,b,*}, Xiaomin Wang ^a, Hongyu Huang ^{c,**}, Yongzhen Wang ^a, Lisheng Deng ^c

^a School of Materials Science and Engineering, Taiyuan University of Technology, Taiyuan, 030024, PR China

^b Institute of Carbon Materials Science, Shanxi Datong University, Datong, 037009, PR China

^c Key Laboratory of Renewable Energy, Guangdong Provincial Key Laboratory of New and Renewable Energy Research and Development, Guangzhou Institute of Energy Conversion, Chinese Academy of Sciences, Guangzhou, 510640, PR China



ARTICLE INFO

Keywords:
LiOH CHS materials
Remarkable heat storage density
Cycle stability
Low-temperature heat storage

ABSTRACT

Lithium hydroxide based chemical heat storage (CHS) materials with high energy density and long storage periods have become the limelight of research for efficient use of low-temperature thermal energy and long-term storage. Herein, we report a novel LiOH composite CHS material with a porous carbon material derived from the zeolite imidazolate framework (ZIF-8) as supporting porous carbon matrix (ZSPCM). The Li/ZSPCM composite exhibits remarkable heat storage density up to 1373.3 kJ kg⁻¹ with low charging temperature and good water adsorption ability owing to the large specific surface area of ZSPCM and well-dispersed small LiOH particles on it, which increase the contact between LiOH and H₂O molecules and concomitant improvement in storage performance. In addition, the storage capacity of this composite material has no significantly degradation after 15 cycles of repeated hydration and dehydration, indicating its excellent cycle stability. And the thermal conductivity of Li/ZSPCM composite also shows a significant improvement over pristine LiOH by virtue of the outstanding thermal conductivity of the ZSPCM. This work develops a promising LiOH CHS material may sheds light on future directions for long period storage of low-temperature heat energy and the further exploitation of ZSPCM.

1. Introduction

A stable energy supply is the cornerstone of the rapid development of society. As a traditional energy source, fossil fuels are not only non-renewable, but also brings environmental problems arise from greenhouse gas emissions. Therefore, the development of renewable energy sources such as solar energy, as well as the recycling technology of industrial residual thermal energy resources, have received considerable research enthusiasm [1,2]. However, these renewable energy and industrial residual thermal energy resources have intermittent as well as unstable characteristics, which causes the contradiction of the mismatch in time, space and intensity of energy recovery and utilization [3,4]. Thence, it is necessary to exploit energy storage technologies to store these unstable energies, and to achieve continuous and stable energy

supply, so as to improve energy utilization efficiency and reduce the impact on the environment.

Metal organic frameworks (MOFs), a type of material that is prepared by connecting inorganic metal ions and organic molecules with adjustable crystal structure, outstanding specific surface area and porosity, has received extensive interest in the area of energy storage technology and gas separation [5–7]. However, MOFs usually exhibit poor resistance to heat and humidity, which greatly limits its practical development and application [8]. Recently, porous carbon materials synthesized by MOFs self-sacrifice have shined in the fields of energy, environment and catalysis due to their superior performance [9,10]. MOF-derived porous carbon materials not only inherit the advantages of MOF's large surface area, high porosity, and excellent customizability, but are also equipped with excellent stability and thermal conductivity characteristics of carbon materials, which makes it show great

* Corresponding author. School of Materials Science and Engineering, Taiyuan University of Technology, Taiyuan 030024, PR China.

** Corresponding author.

E-mail addresses: zhaojianguo@sxtdx.edu.cn (J. Zhao), huanghy@ms.giec.ac.cn (H. Huang).

Nomenclature

A	pre-exponential factor
d _p	pore diameter (nm)
E _a	activation energy (kJ mol ⁻¹)
f(α)	function of dehydration conversion
R	universal gas constant [J (mol K) ⁻¹]

Abbreviations

BET	Brunauer-Emmett-Teller
CHS	chemical heat storage
LiOH	lithium hydroxide
MOF	metal organic framework
RH	relative humidity (%)
SEM	scanning electron microscope
STA	synchronous thermal analyzer
XRD	X-ray diffraction
ZIF-8	zeolite imidazolate framework
ZSPCM	zeolite imidazolate framework derived supporting porous carbon matrix

Greek symbols

β	heating rate [K min ⁻¹]
---	-------------------------------------

application potential compared with traditional carbon materials as supporting porous matrix [11,12]. Compared with its wide application in other fields, the application of MOF-derived porous carbon materials in heat storage is relatively scarce, especially in the field of chemical heat storage [13].

The thermal energy storage technology, which can fully overcome the timing conflict between energy supply and demand, has shown great practical application value in the field of high-efficiency utilization of renewable energy [14,15]. Sensible heat storage technology, latent heat storage technology and chemical heat storage technology are the three most common heat storage technologies [16]. Compared with the first two methods, the chemical heat storage technology is not only equipped with seasonal or long-term storage capacity that can store solar energy in summer and use it in winter, but also has the advantages of large heat storage capacity and negligible heat loss, which makes it the limelight of thermal energy storage [17,18].

In a various types of chemical heat storage technologies, salt hydrates and their derivatives based chemical heat storage (CHS) materials have particularly received considerable research interest arise from the availability and low cost of water, as well as the high safety and the simple hydration→dehydration reaction mechanism [19–21]. However, the application temperature of most heat storage materials is relatively high, so the effective use of abundant low-temperature thermal energy (such as industrial residual thermal energy resources and solar energy) has become a shortcoming in the large-scale practical application of CHS technology [22,23]. In this context, lithium hydroxide (LiOH) with the merits of low reaction temperature, excellent storage performance and no side reactions has become a competitive candidate in the field of making full use of low-temperature thermal energy [24–26]. Nevertheless, pristine LiOH still suffers from low thermal conductivity and hydration rate, agglomeration and poor cycle stability, which greatly increases the gap with practical applications as a CHS material [27]. Therefore, how to simultaneously improve the thermal conductivity, heat storage capacity, hydration rate, and cycle stability of LiOH·CHS composites, which are closely related to practical applications, is still a thorny challenge.

In this work, we report a novel LiOH composite CHS material with a porous carbon derived from the zeolite imidazolate framework (ZIF-8) as supporting porous carbon matrix (ZSPCM) for low grade heat storage

and utilization, as shown in Fig. 1. By taking the advantages of large specific surface area and abundant pore structure of ZSPCM, this Li/ZSPCM composite exhibits remarkable heat storage density with low charging temperature and good water adsorption ability as a result of the well-dispersed small LiOH particles on the surface of ZSPCM. Moreover, the heat storage capacity of this Li/ZSPCM composite material did not significantly degrade after 15 cycles of repeated hydration and dehydration, which shows that it has excellent cycle stability. And the thermal conductivity of Li/ZSPCM composite was also greatly improved compared to pristine LiOH, which significantly improves its exploitation prospects.

2. Experimental methodology

2.1. Raw materials and reagents

Zinc nitrate hexahydrate ($\text{Zn}(\text{NO}_3)_2 \cdot 6\text{H}_2\text{O}$, 98%), 2-methylimidazole (98%), Lithium hydroxide monohydrate ($\text{LiOH}\cdot\text{H}_2\text{O}$, 98%) were purchased from Sigma-Aldrich Co., Ltd and used directly as received.

2.2. Synthesis of ZIF-8 derived supporting porous carbon matrix

ZIF-8 derived supporting porous carbon matrix was prepared using the modified literature procedure [28]. Typically, 100 mL methanol containing 1.468 g of $\text{Zn}(\text{NO}_3)_2 \cdot 6\text{H}_2\text{O}$ was added dropwise to vigorously stirred 100 mL methanol containing 1.621 g of 2-methylimidazole, and the mixture was continuously stirred at 27 °C for 60 min after the dripping was completed. Then the mixture was aged for 4 h, and the mixture was centrifuged and washed with methanol at least 4 times. After drying in vacuum at 60 °C for 15 h, the obtained ZIF-8 powder was heated to 700 °C at a heating rate of 3 °C min⁻¹ and kept for 3 h under N₂ atmosphere. After cooling down to 27 °C at a cooling rate of 3 °C min⁻¹, the resulting black powder was immersed in HCl (2 M) for 10 h to remove the zinc component in the sample. Finally, the crude product was filtered and washed with deionized water until it was neutral, and the supporting porous carbon matrix derived from ZIF-8 was obtained after dried at 70 °C for 10 h, denoted as ZSPCM(700). For comparison, ZSPCM(600) and ZSPCM(800) were prepared by similar steps, except that the carbonization temperature was changed to 600 °C and 800 °C, respectively.

2.3. Preparation of LiOH chemical heat storage composites

The prepared ZSPCM(700) powder (100 mg) was added to 50 mL of deionized water with different dehydrated LiOH contents and stirred at 27 °C for 0.5 h. The mixture was then transferred into a 100 mL Teflon-lined stainless steel autoclave and kept in an oven at 150 °C for 10 h. After the autoclave was cooled to 27 °C, the resulting black solution was dried at 100 °C for 5 h to obtain a completely dehydrated target LiOH·CHS composite material. The target products with different LiOH content (30 wt%, 40 wt%, 50 wt%, 60 wt%) were denoted as Li/ZSPCM-30, Li/ZSPCM-40, Li/ZSPCM-50 and Li/ZSPCM-60, respectively. For comparison, Li/ZSPCM(600)-50 and Li/ZSPCM(800)-50 were prepared by similar steps, except that the ZSPCM was changed to ZSPCM(600) and ZSPCM(800), respectively. And the preparation process is shown in Fig. 2.

2.4. Characterizations

The scanning electron microscope (SEM) was performed on Merlin Compact (Carl Zeiss, Germany). X-ray diffraction (XRD) was performed on a D8 advance (Bruker, Germany). Raman spectrum was procured by invia (Renishaw, England). The specific surface area and pore size distribution isotherms were procured on ASAP 2460 (Micromeritics, USA). The hydration experiment of the material and the water absorption capacity under different relative humidity (RH) were measured by a

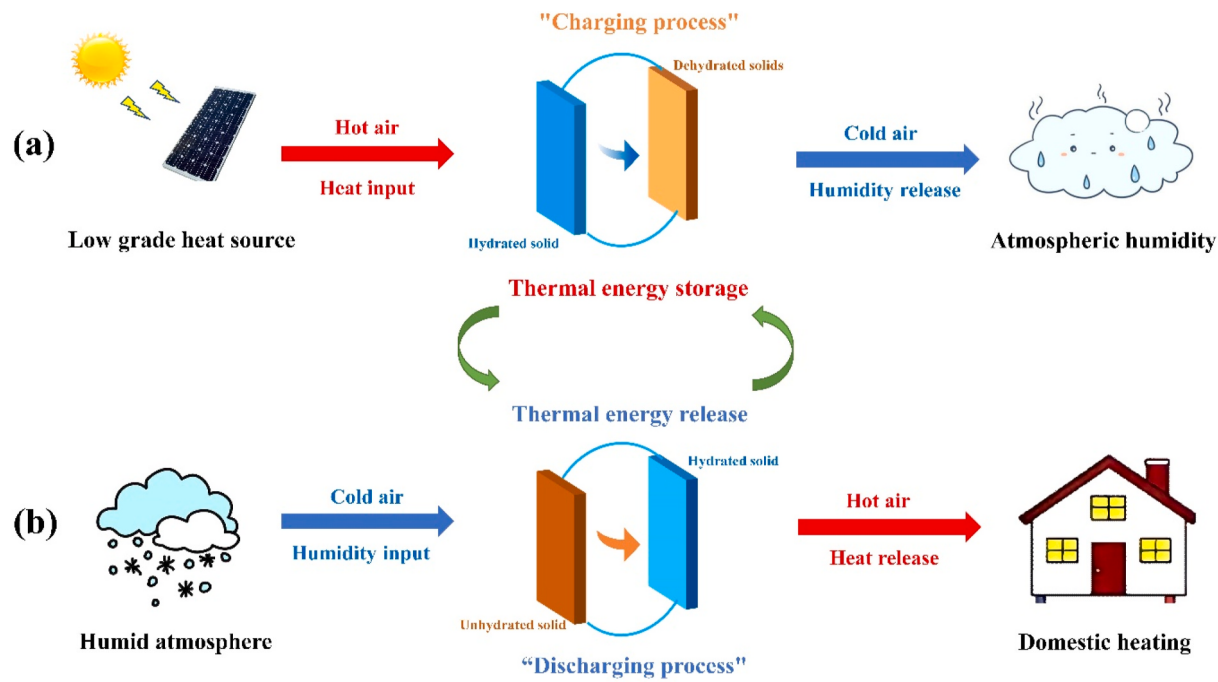


Fig. 1. Working diagram of the Li/ZSPCM composite for low grade heat storage and utilization. (a) Charging process: dehydrate the Li/ZSPCM composite through low grade heat source. (b) Discharging process: hydrate the Li/ZSPCM composite for indoor heating.

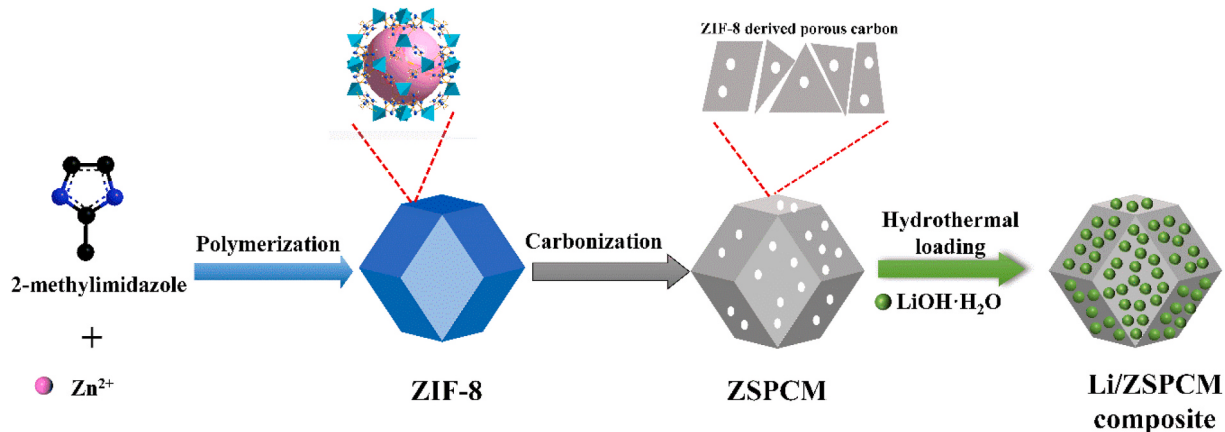


Fig. 2. Schematic demonstration of the preparation process of Li/ZSPCM.

constant temperature and humidity system (YNK/TH-150, UNIQUE Environmental Test Equipment, China), wherein the sample is kept at 30 °C for 3 h in the RH range of 50%–80% to reach water absorption equilibrium. The thermal conductivity was procured by a Hot Disk TPS2500S (Hot Disk, Sweden). The activation energy of dehydration reaction of pristine LiOH and Li/ZSPCM(700)-50 was calculated according to **Equation 1** based on the heating rate of 5, 10, 15 and 20 K min⁻¹ [29].

$$\ln\left(\frac{\beta}{T^2}\right) = \ln\frac{R}{E_a} \frac{A}{f(\alpha)} - \frac{E}{R} \frac{1}{T}$$

where E_a is activation energy, β is heating rate, T is temperature, R is universal gas constant, A is the pre-exponential factor, $f(\alpha)$ is the function of dehydration conversion, respectively.

The heat storage performance test of the material was completed by the following steps: First, the samples were placed at 30 °C and a RH of 80% for 3 h to fully hydrated. After hydration, the material's dehydration enthalpy change, temperature and relative mass change during

dehydration were measured by a synchronous thermal analyzer (STA; 449F5, NETZSCH, Germany) at a heating rate of 5 °C min⁻¹ from 30 °C to 200 °C for 37 min by using N₂ as the carrier gas with a flow rate of 50 mL min⁻¹.

3. Results and discussion

3.1. Morphologies, chemical structure and pore properties

The morphologies of ZIF-8, ZSPCM(700) and Li/ZSPCM(700)-50 composite were observed by SEM. It can be seen from Fig. 3a that ZIF-8 shows a smooth surface with uniform particle size and regular shape. And its average particle size is between 50 and 100 nm with slightly agglomerated. It can be seen from Fig. 3b that the surface of the ZSPCM(700) obtained after carbonization at 700 °C become rougher, but maintain the original morphology of the ZIF-8 and excellent porous structure, and the particle size is also slightly reduced and has better dispersibility, which significantly reduces the agglomeration

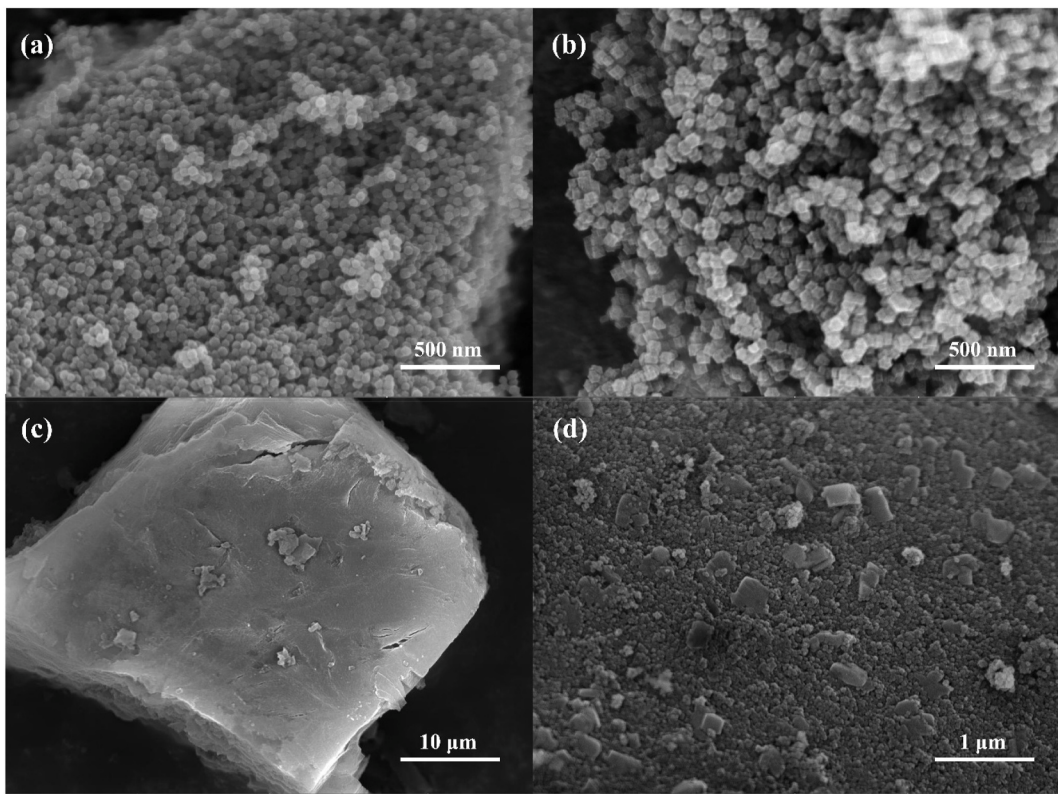


Fig. 3. SEM images of (a) ZIF-8, (b) ZSPCM(700), (c) pristine LiOH, (d) Li/ZSPCM(700)-50.

phenomenon. **Fig. 3c** shows that the particle size of pristine LiOH is relatively large and exhibits obvious agglomeration, which is harmful to its full contact and reaction with H₂O molecules during the hydration process. Moreover, it can be seen from **Fig. 3d** that in the Li/ZSPCM(700)-50 composite, the particle size of LiOH has become significantly smaller and well dispersed on the surface of the ZSPCM(700) without obvious structural change compared with ZSPCM(700), which is beneficial to the uniform dispersion of LiOH and better contact and react with H₂O molecules during the hydration process.

From the XRD patterns of ZIF-8 crystal and ZSPCM (**Fig. 4a**), it can be seen that the positions of the diffraction peaks are consistent with those in the literature, indicating that the ZIF-8 crystal has been successfully synthesized, and the diffraction peaks of ZIF-8 are relatively sharp, indicating its high crystallinity [30]. After ZIF-8 is heated and carbonized to ZSPCM at different temperatures, a broad peak appears at 24.6°, which is attributed to the characteristic peak of amorphous graphitic carbon, and an inconspicuous diffraction peak also appears at 44°,

corresponding to the characteristic peak of graphite, indicating that all ZSPCMs obtained after carbonization have a certain degree of graphitization [31]. Different carbonization temperatures have a great impact on the degree of graphitization of carbon elements. In order to analyze the state of carbon in the ZSPCMs, the Raman spectra of the materials under different temperatures were tested, as shown in **Fig. 4c**. In the Raman spectrum of the samples, the peak at 1332 cm⁻¹ corresponds to amorphous carbon or defective graphitic carbon, which is represented by D band, and the peak at 1590 cm⁻¹ corresponds to graphitized carbon, which is represented by G band. It is obvious that the I_D/I_G value of ZSPCM(700) (0.93) is higher than that of ZSPCM(600) (0.86) and ZSPCM(800) (0.88), which indicates that ZSPCM(700) has a higher degree of defects [32]. The large number of defects generated after carbonization is more conducive to the uniform dispersion of LiOH on ZSPCM and the full hydration of LiOH as well as consequently increases the heat storage capacity, which makes ZSPCM(700) the optimum candidate as a support matrix. Moreover, it can be clearly seen from

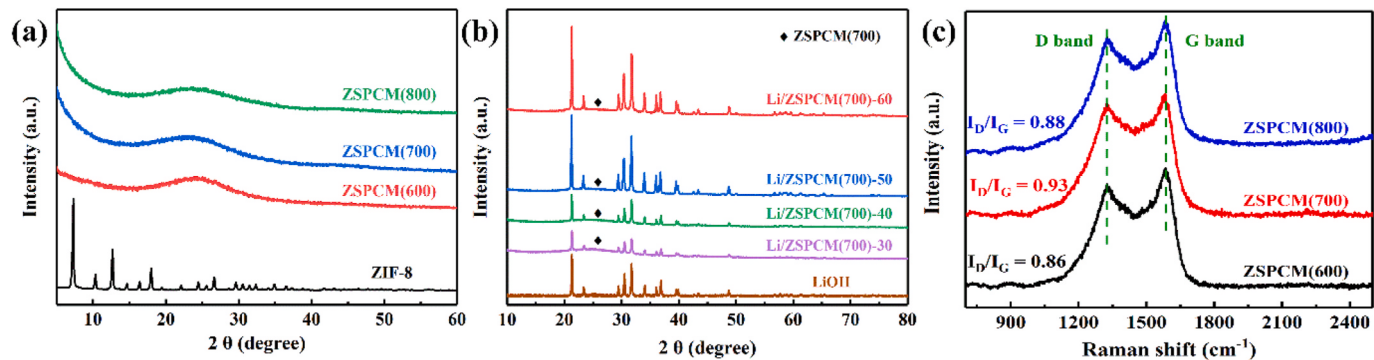


Fig. 4. (a) XRD patterns of ZIF-8 and ZSPCM with different carbonization temperature. (b) XRD patterns of pristine LiOH and Li/ZSPCM(700)-x composites with different LiOH content. (c) Raman spectra of ZSPCM with different carbonization temperature.

Fig. 4b that all Li/ZSPCM(700)-x composites exhibit the characteristic diffraction peaks of LiOH which consistent with those reported in the literature, and the amorphous carbon diffraction peaks attributed to ZSPCM(700) can also be clearly observed at 24.6° , which all proved the successful composite of LiOH and ZSPCM(700) [33].

The pore characteristics of ZIF-8, ZSPCMs, Li/ZSPCM(700)-50 and pristine LiOH were measured by nitrogen adsorption-desorption experiment. It can be seen from **Fig. 5a** that the N_2 adsorption-desorption isotherms of ZSPCM(700) and Li/ZSPCM(700)-50 show a vertical upward trend near the relative pressure (P/P_0) of 0, and there is no obvious hysteresis loop between the (P/P_0) of 0–1, indicating that they are both typical Type I isotherms and there are a lot of micropores in the material [34]. The pore-size distribution curve (**Fig. 5b**) shows that all the tested samples have similar pore size distributions and the pore sizes are mainly distributed in before 2 nm, which proves that the load of LiOH on ZSPCM(700) does not change the original micropore feature of ZSPCM(700). And the corresponding BET specific surface area, total pore volume and average pore size of all test samples are summarized in **Table 1**. It can be seen that compared to ZSPCM(600) ($510.1 \text{ m}^2 \text{ g}^{-1}$) and ZSPCM(800) ($794.7 \text{ m}^2 \text{ g}^{-1}$), ZSPCM(700) shows the largest specific surface area of $890.2 \text{ m}^2 \text{ g}^{-1}$, which makes it a promising supporting porous matrix for loading nanoscale LiOH particles. Furthermore, all Li/ZSPCM(700) samples show a larger specific surface area than pristine LiOH ($17.4 \text{ m}^2 \text{ g}^{-1}$). It can be concluded from the above results that ZSPCM(700) with a larger specific surface area and abundant pore structure not only promotes the dispersion of LiOH with a smaller particle size on its surface, but also alleviates the agglomeration of LiOH, which allows LiOH and H_2O molecules to be more fully contact and react as well as reduce the activation energy of the reaction, and ultimately significantly improve the heat storage performance of the Li/ZSPCM(700)-x composite [33].

3.2. Water adsorption capacity of LiOH and Li/ZSPCM(700)-x at different RH

In the area of thermochemical heat storage, the water absorption capacity of CHS materials under different conditions is directly related to the degree of hydration reaction, which means that it has a dramatic impact on the heat storage capacity of the material. In this context, the water adsorption capacities of Li/ZSPCM(700) with different LiOH content and pristine LiOH (100%) at different RH were investigated and the corresponding hydration conversion rate of each sample under different RH are shown in **Table 2**. As shown in **Fig. 6a**, compared to pristine LiOH with a larger particle size, all Li/ZSPCM(700)-x

Table 1
Pore characteristics of ZIF-8, ZSPCMs, Li/ZSPCM(700)-x and LiOH.

Samples	$S_{\text{BET}} (\text{m}^2 \text{ g}^{-1})$	Total pore volume ($\text{cm}^3 \text{ g}^{-1}$)	Average pore size (nm)
ZIF-8	1293.1	0.66	2.04
ZSPCM(600)	510.1	0.88	6.11
ZSPCM(700)	890.2	1.05	4.74
ZSPCM(800)	794.7	0.98	3.64
Li/ZSPCM(700)-30	699.2	0.94	5.51
Li/ZSPCM(700)-40	598.9	0.82	5.44
Li/ZSPCM(700)-50	486.2	0.64	5.29
Li/ZSPCM(700)-60	303.6	0.26	3.45
LiOH	17.4	0.08	1.78

composites exhibit a higher water absorption capacity due to their larger specific surface area and well-dispersed smaller nano-scale LiOH particles on it, which together enhance the contact and react between LiOH and H_2O molecules and increase the degree of hydration [35]. In addition, when the LiOH content gradually increases from 30% to 50%, the water absorption content of the composites under each RH increases correspondingly. But when the LiOH content increases from 50% to 60%, the water absorption content of the composite material under each RH decreases. This may be due to the high content of LiOH in Li/ZSPCM(700)-60, which causes serious accumulation of LiOH on the surface of Li/ZSPCM(700)-60, resulting in an increase in the particle size of LiOH particles as well as poor dispersion on the surface of Li/ZSPCM(700)-60, ultimately resulting in a decrease in its water absorption capacity [36]. This conclusion is also confirmed by SEM (**Fig. 6b**) and partially explains the reason for the best thermal storage performance of Li/ZSPCM(700)-50.

3.3. Heat storage performance and cycling stability

In order to find out the optimal carbonization temperature of ZSPCM, the heat storage performance of composite materials with the same LiOH content under different carbonization temperatures were investigated. It can be seen from **Fig. 7** and **Fig. 8d** that compared with Li/ZSPCM(600)-50 (830.8 kJ kg^{-1}) and Li/ZSPCM(800)-50 (880.1 kJ kg^{-1}), Li/ZSPCM(700)-50 has the largest heat storage density of $1373.3 \text{ kJ kg}^{-1}$ arise from the larger specific surface area and higher defect degree of ZSPCM(700), which improves the dispersibility of LiOH

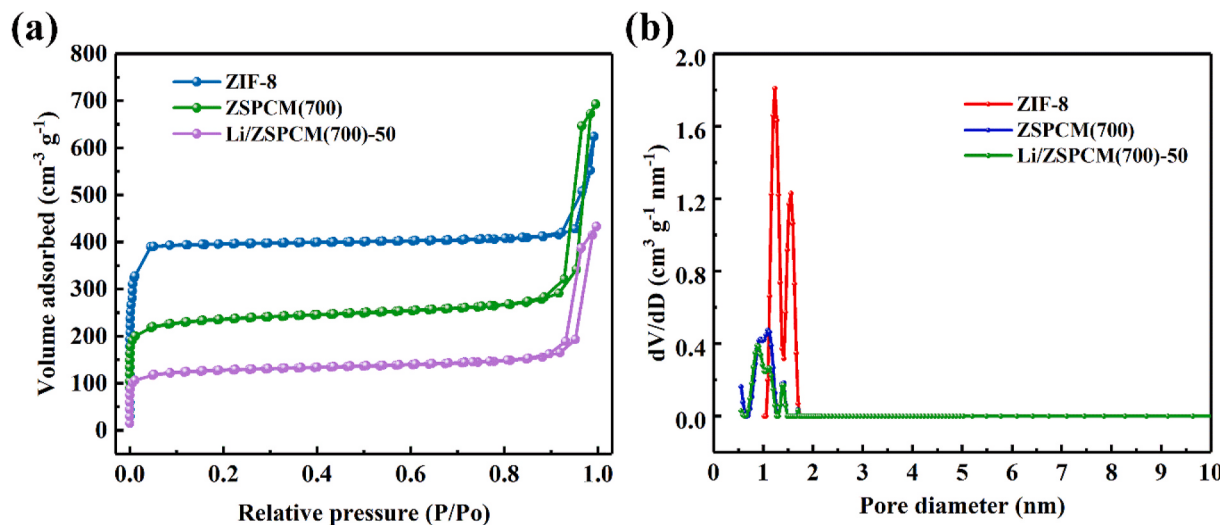


Fig. 5. (a) N_2 adsorption-desorption isotherms. (b) Pore size distribution curves of ZIF-8, ZSPCM(700) and Li/ZSPCM(700)-50 composite.

Table 2

The hydration conversion rate of each sample under different RH conditions.

Samples	Hydration conversion rate at 50% RH (%)	Hydration conversion rate at 60% RH (%)	Hydration conversion rate at 70% RH (%)	Hydration conversion rate at 80% RH (%)
Li/ZHPCM(700)-30	37.1	40.7	43.9	45.8
Li/ZHPCM(700)-40	38.5	41.6	44.5	47.7
Li/ZHPCM(700)-50	41.2	44.5	47.6	50.9
Li/ZHPCM(700)-60	40.6	43.3	45.8	48.3
pristine LiOH (100%)	36.7	39.4	40.7	44.5

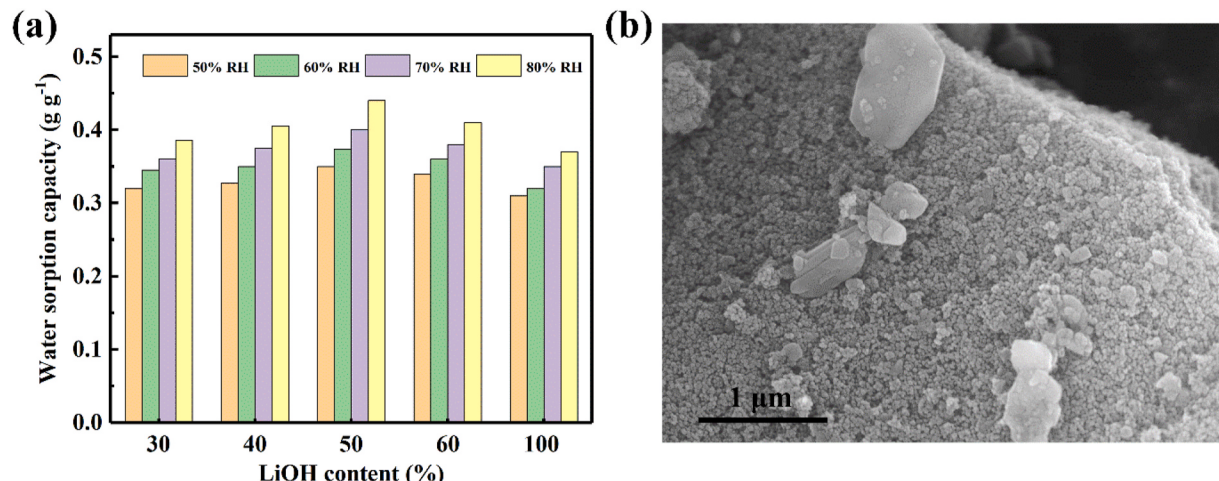


Fig. 6. (a) Water adsorption capacity of pristine LiOH (100%) and Li/ZSPCM(700)-x composites with different LiOH content under different RH at 30 °C. (b) SEM image of Li/ZSPCM(700)-60.

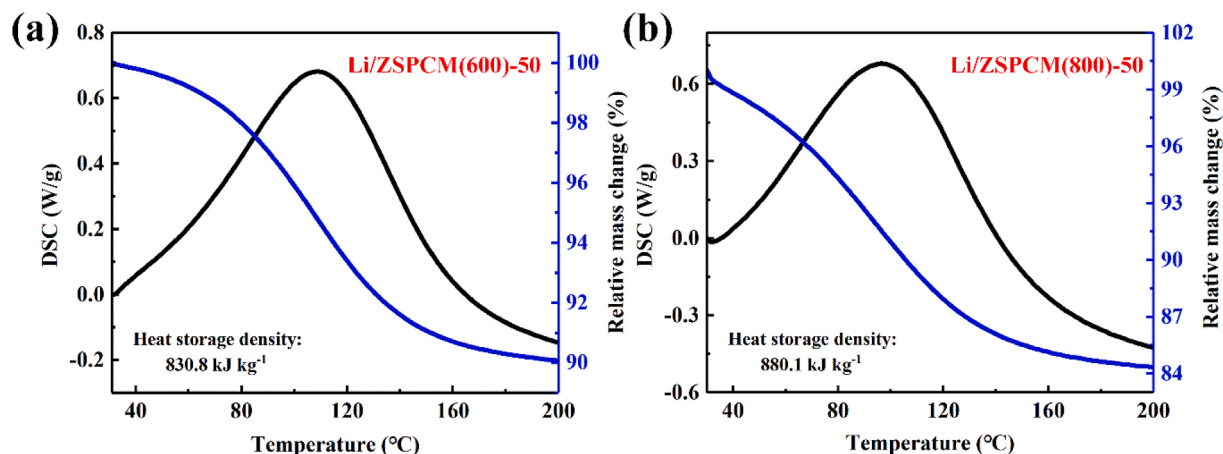


Fig. 7. STA traces of (a) Li/ZSPCM(600)-50, (b) Li/ZSPCM(800)-50.

particles and the effect of hydration reaction, thus promoting the improvement of the heat storage performance of composite materials. This conclusion is also confirmed by BET and Raman.

After determining the best ZSPCM, the storage capability of pristine LiOH and Li/ZSPCM(700)-x composites with different LiOH content were also investigated. As shown in Fig. 8a, the heat storage density of pristine LiOH is only 494 kJ kg^{-1} attribute to the insufficient hydration of LiOH into $\text{LiOH-H}_2\text{O}$ during the hydration process, which may originate from the large particle size of pristine LiOH. This result demonstrates that increasing the degree of hydration of LiOH is pivotal for

enhancing the storage capacity of LiOH CHS materials. As shown in Fig. 8b-e, when LiOH is successfully loaded on ZSPCM(700), the heat storage density of Li/ZSPCM(700)-x composites with different LiOH contents is significantly higher than that of pristine LiOH because of the larger specific surface area and well-dispersed smaller nano-scale LiOH particles on it, which increases the contact between LiOH and water molecules and concomitant improvement in heat storage capacity [35]. This conclusion is also supported by SEM and BET results. It is worth noting in Fig. 8f that the heat storage density of the composite material is positively correlated with the LiOH content from 30% to 50%, and

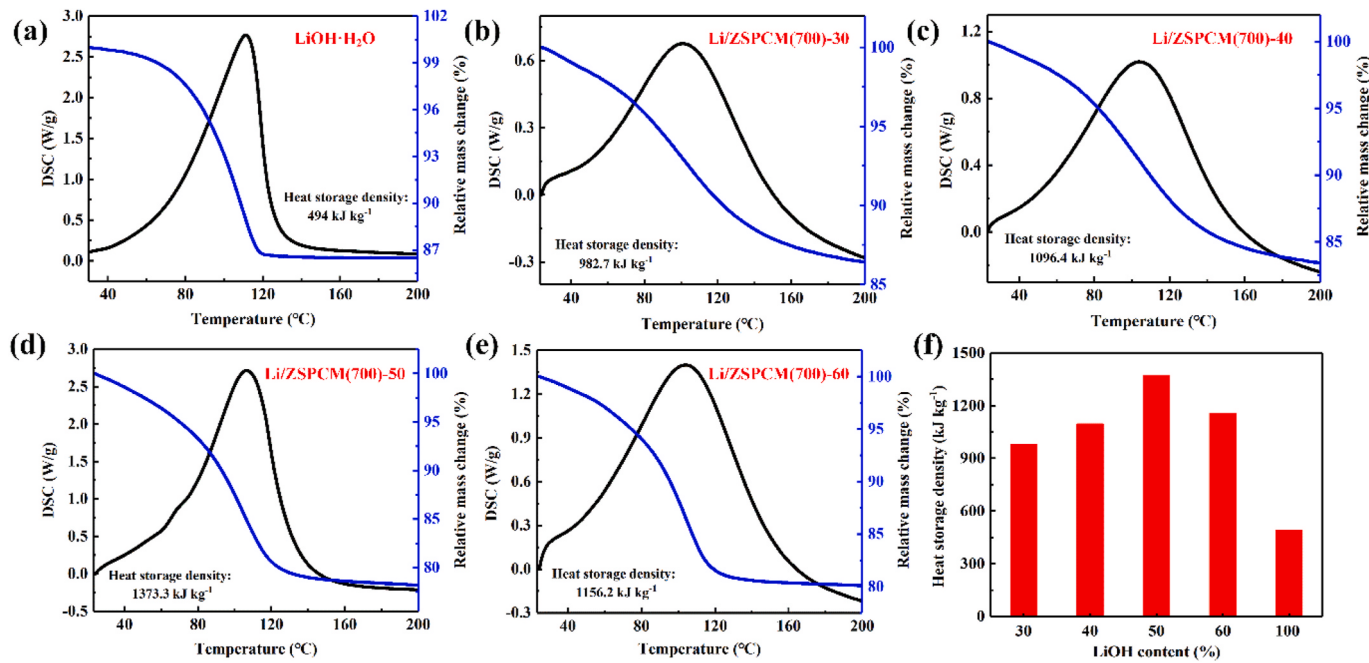


Fig. 8. STA traces of (a) pristine LiOH-H₂O and (b–e) Li/ZSPCM(700)-x composites with different LiOH content. (f) The relationship between heat storage density and LiOH content of Li/ZSPCM(700)-x composites.

Li/ZSPCM(700)-50 exhibits the highest heat storage density of 1373.3 kJ kg⁻¹ normalized by LiOH content, which is 2.8 times that of pristine LiOH (494 kJ kg⁻¹). However, when the LiOH content increases from

50% to 60%, the heat storage density of the composite decreases. This may come from the excessively high LiOH content in the Li/ZSPCM(700)-60 that caused the LiOH to accumulate on its surface, which

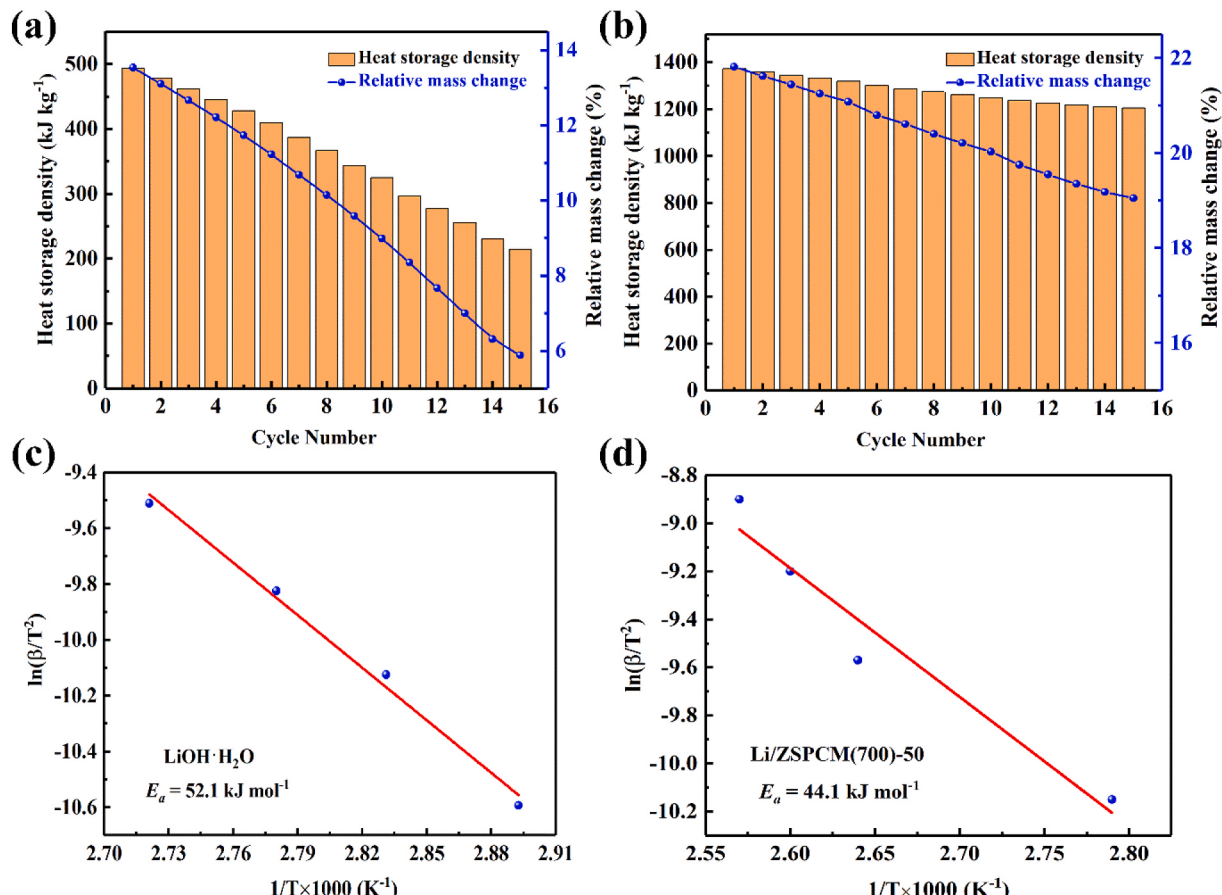


Fig. 9. Cycling performance and the activation energy of dehydration reaction of (a, c) pristine LiOH (b, d) Li/ZSPCM(700)-50.

results in the increase of the particle size of the LiOH particles and poor dispersion on the surface of the Li/ZSPCM(700)-60, and ultimately reduces the degree of hydration of the LiOH and causes a decrease in the heat storage density [29]. This result is consistent with the result of the water absorption capacity test, which further proves the close relationship between the degree of hydration of LiOH and the heat storage capacity of the heat storage material. The above results show that Li/ZSPCM(700)-50 with the best heat storage density and excellent hydration performance has shown great potential in the practical application of low-temperature thermochemical energy storage.

In addition to heat storage capacity, the cycle stability of CHS materials is also a vital indicator for evaluating their practical application potential. Therefore, the cycle stability of Li/ZSPCM(700)-50 with the best heat storage performance and pristine LiOH as a comparison were investigated (Fig. 9). Each complete cycle included the hydration and dehydration process under the same conditions as the STA, in which the normalized relative mass change was used to represent the water absorption capacity in each cycle. As shown in Fig. 9a–b, the heat storage density and water absorption capacity of the two materials decrease as the number of cycles increase but shows different degrees of decline. The heat storage density and relative mass change of pristine LiOH (Fig. 9a) showed a relatively drastic decline after 15 cycles due to the growing phenomenon of aggregation, in which the heat storage density decreased from 494 kJ kg^{-1} to 214.7 kJ kg^{-1} by 56.5%; and the relative mass change decreased from 13.54% to 5.88% by 56.6%. In contrast, the reduction of various parameters of Li/ZSPCM(700)-50 (Fig. 9b) was relatively gentle as a result of relatively lighter aggregation of LiOH particles, in which heat storage density decreased from $1373.3 \text{ kJ kg}^{-1}$ to $1205.4 \text{ kJ kg}^{-1}$ by 12.2% and the relative mass change decreased from 21.82% to 19.05% by 12.9%. It is also worth noting in Fig. 9c–d that the activation energy required by Li/ZSPCM(700)-50 (44.1 kJ mol^{-1}) during the dehydration process is much lower than that of pristine LiOH (52.1 kJ mol^{-1}) due to the larger specific surface area and well-dispersed smaller nano-scale LiOH particles on the surface of ZSPCM(700), which makes the hydration reaction of Li/ZSPCM(700)-50 less hindered, and ultimately leads to a lighter attenuation of Li/ZSPCM(700)-50 after cycling. The above results demonstrate that Li/ZSPCM(700)-50 exhibits better cycle stability than pristine LiOH, which makes it the optimum candidate for long-term low temperature heat storage.

Furthermore, it is worth noting that thermal conductivity is also inseparable from the performance of CHS materials in actual heat and mass transfer. As shown in Fig. 10a, the thermal conductivity of all Li/

ZSPCM(700)-x composites shows a significant improvement over pristine LiOH, which is ascribed to the excellent thermal conductivity of the supporting porous carbon matrix. Moreover, the thermal conductivity of Li/ZSPCM(700)-30 can reach up to $1.26 \text{ W m}^{-1} \text{ K}^{-1}$, which is 183% higher than that of pristine LiOH ($0.69 \text{ W m}^{-1} \text{ K}^{-1}$). It can be seen from Fig. 10b that although the thermal conductivity of the composite material is inversely proportional to the heat storage density, while Li/ZSPCM(700)-50 achieves the best heat storage density and its thermal conductivity ($0.98 \text{ W m}^{-1} \text{ K}^{-1}$) is also increases by 142% compared to pristine LiOH, which further proves that Li/ZSPCM(700)-50 is the optimum candidate among all tested samples. On the other hand, Table 3 also shows that compared with the different CHS composite materials, Li/ZSPCM(700)-50 with relatively low dehydration temperature has shown significant progress in the parameters representing the storage performance of CHS composite materials [36–41]. Therefore, a conclusion can be drawn from the above results that Li/ZSPCM(700)-50 composite material, which not only equipped with high heat storage density and outstanding hydration ability, but also exhibits remarkable cyclic stability and thermal conductivity, has great practical application potential in the field of long-term storage of low-temperature thermal energy.

4. Conclusion

In summary, the Li/ZSPCM(700) composite has been proven to be a great CHS material with excellent storage capacity and water adsorption ability. The morphologies, chemical structure and pore properties of ZSPCM(700) and Li/ZSPCM(700)-x composite have been thoroughly characterized and investigated. Water adsorption capacity investigation is carried out to evaluate hydration performance of LiOH and Li/ZSPCM(700)-x. Key indicators representing heat storage performance such as heat storage density, cycling stability, activation energy as well as thermal conductivity is also researched. The following conclusions are drawn through observation:

- ZSPCM(700) with the largest specific surface area of $890.2 \text{ m}^2 \text{ g}^{-1}$ and abundant pore structure as well as higher degree of defects makes it an optimum supporting porous matrix for loading nanoscale LiOH particles.
- Li/ZSPCM(700)-50 composite exhibits the best hydration conversion rate under different RH compared with pristine LiOH and other four test samples owing to the large specific surface area and well-

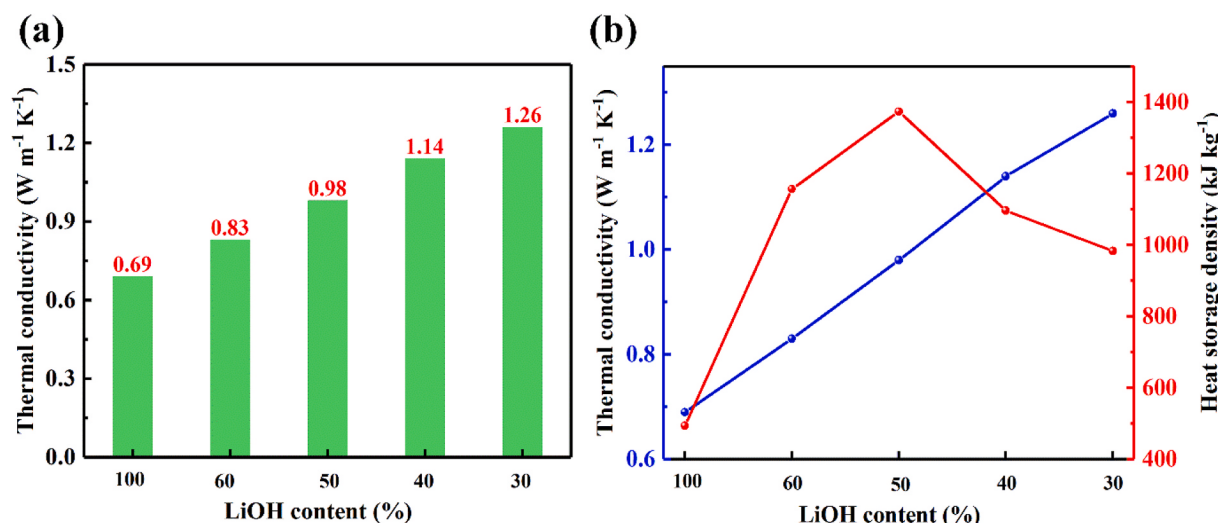


Fig. 10. (a) Thermal conductivity (b) thermal conductivity versus heat storage density of pristine LiOH (100%) and Li/ZSPCM(700)-x composites with different LiOH content.

Table 3

Comparison of a series of heat storage parameters of different CHS composite materials.

CHS composite material	Dehydration temperature (°C)	Max water absorption capacity (g g ⁻¹)	Heat storage density (kJ kg ⁻¹)	Thermal conductivity (W m ⁻¹ .K ⁻¹)	Ref.
Ca(OH) ₂ /ZrO(NO ₃) ₂	310	0.25	1125	\	[37]
Mg(OH) ₂ /GO	350	\	765	1.23	[38]
SrCl ₂ /silica gel	125	0.34	1301.3	\	[39]
MgSO ₄ -zeolite 13×	150	0.27	632	\	[36]
SrBr ₂ /expanded graphite	250	0.34	850	5.57	[40]
LiBr/activated carbon	120	0.32	939.6	\	[41]
Li/ZSPCM(700)-50	105	0.44	1373.3	0.98	This work

dispersed smaller nano-scale LiOH particles on the surface of ZSPCM (700).

- Compared with pristine LiOH, Li/ZSPCM(700)-50 composite not only has better the heat storage capacity (max. 1373.3 kJ kg⁻¹) and thermal conductivity up to 0.98 W m⁻¹ K⁻¹, but also exhibits outstanding cycle performance for 15 cycles of consecutive hydration and dehydration without significant degradation and much lower activation energy of 44.1 kJ mol⁻¹ during the dehydration process.

The result indicates that the Li/ZSPCM(700)-x composites, combining high heat storage density and outstanding hydration ability with excellent cycle stability and thermal conductivity, is not only a candidate with great potential for efficient use of low-temperature thermal energy and long-term storage, but also points out a new direction for the further application of CHS material to indoor heating and addresses the global energy crisis in the future. Nevertheless, in the actual industrial application of Li/ZSPCM(700)-x, it is still necessary to overcome the problem that the environmental RH may not be able to fully hydrate the material and low exothermic temperature caused by inevitable heat transfer loss, which is also a key direction that the reactor composed of Li/ZSPCM(700)-x needs to be improved.

CRediT authorship contribution statement

Xiangyu Yang: Conceptualization, Formal analysis, Investigation, Writing – original draft. **Shijie Li:** Resources, Data curation, Writing – review & editing. **Jianguo Zhao:** Supervision. **Xiaomin Wang:** Visualization, and. **Hongyu Huang:** Visualization. **Yongzhen Wang:** Validation. **Lisheng Deng:** Visualization.

Declaration of competing interest

The authors declare that they have no known competing financial interests or personal relationships that could have appeared to influence the work reported in this paper.

Acknowledgements

The authors appreciate the support from National Natural Science Foundation of China (Grant No. 52071192), Key Research Program of Frontier Sciences, CAS, (Grant No. QYZDY-SSW-JSC038), Key-Area Research and Development Program of Guangdong Province (Grant No. 2019B11020900).

References

- A.J. Carrillo, J. González-Aguilar, M. Romero, J.M. Coronado, Solar energy on demand: a review on high temperature thermochemical heat storage systems and materials, *Chem. Rev.* 119 (2019) 4777–4816.
- M. Sevilla, R. Mokaya, Energy storage applications of activated carbons: supercapacitors and hydrogen storage, *Energy Environ. Sci.* 7 (2014) 1250–1280.
- A. Gil, M. Medrano, I. Martorell, A. Lázaro, P. Dolado, B. Zalba, L.F. Cabeza, State of the art on high temperature thermal energy storage for power generation. Part 1—concepts, materials and modelling, *Renew. Sustain. Energy Rev.* 14 (2010) 31–55.
- R.-J. Clark, A. Mehrabadi, M. Farid, State of the art on salt hydrate thermochemical energy storage systems for use in building applications, *Journal of Energy Storage* 27 (2020), 101145.
- Introduction to metal–organic frameworks, *Chem. Rev.* 112 (2012) 673–674.
- G. Zhong, D. Liu, J. Zhang, The application of ZIF-67 and its derivatives: adsorption, separation, electrochemistry and catalysts, *J. Mater. Chem. B* 6 (2018) 1887–1899.
- R. Kumar, K. Jayaramulu, T.K. Maji, C.N.R. Rao, Hybrid nanocomposites of ZIF-8 with graphene oxide exhibiting tunable morphology, significant CO₂ uptake and other novel properties, *Chem. Commun.* 49 (2013) 4947–4949.
- L.G. Gordeeva, Y.D. Tu, Q. Pan, M.L. Palash, B.B. Saha, Y.I. Aristov, R.Z. Wang, Metal–organic frameworks for energy conversion and water harvesting: a bridge between thermal engineering and material science, *Nanomater. Energy* 84 (2021), 105946.
- J. Wang, Y. Wang, H. Hu, Q. Yang, J. Cai, From metal–organic frameworks to porous carbon materials: recent progress and prospects from energy and environmental perspectives, *Nanoscale* 12 (2020) 4238–4268.
- X. Liu, X. Wang, F. Kapteijn, Water and metal–organic frameworks: from interaction toward utilization, *Chem. Rev.* 120 (2020) 8303–8377.
- M.F. de Lange, K.J.F.M. Verouden, T.J.H. Vlugt, J. Gascon, F. Kapteijn, Adsorption-driven heat pumps: the potential of metal–organic frameworks, *Chem. Rev.* 115 (2015) 12205–12250.
- L. Garzón-Tovar, J. Pérez-Carvajal, I. Imaz, D. Maspoch, Composite salt in porous metal–organic frameworks for adsorption heat transformation, *Adv. Funct. Mater.* 27 (2017) 1606424.
- A. Elsayed, E. Elsayed, R. Al-Dadah, S. Mahmoud, A. Elshaer, W. Kaialy, Thermal energy storage using metal–organic framework materials, *Appl. Energy* 186 (2017) 509–519.
- S. Koohi-Fayegh, M.A. Rosen, A review of energy storage types, applications and recent developments, *Journal of Energy Storage* 27 (2020), 101047.
- S. Chavan, V. Guntapure, D. Arumuga Perumal, Characterization of linear low-density polyethylene with graphene as thermal energy storage material, *Mater. Res. Express* 6 (2019), 065511.
- G. Alva, Y. Lin, G. Fang, An overview of thermal energy storage systems, *Energy* 144 (2018) 341–378.
- S. Bennici, T. Polimann, M. Ondarts, E. Gonze, C. Vaultor, N. Le Pierrès, Long-term impact of air pollutants on thermochemical heat storage materials, *Renew. Sustain. Energy Rev.* 117 (2020), 109473.
- P.A.J. Donkers, L.C. Sögütoglu, H.P. Huinink, H.R. Fischer, O.C.G. Adan, A review of salt hydrates for seasonal heat storage in domestic applications, *Appl. Energy* 199 (2017) 45–68.
- A. Jabbari-Hichri, S. Bennici, A. Auroux, Enhancing the heat storage density of silica–alumina by addition of hygroscopic salts (CaCl₂, Ba(OH)₂, and LiNO₃), *Sol. Energy Mater. Sol. Cell.* 140 (2015) 351–360.
- E. Mastronardo, L. Bonaccorsi, Y. Kato, E. Piperopoulos, M. Lanza, C. Milone, Strategies for the enhancement of heat storage materials performances for MgO/H₂O/Mg(OH)₂ thermochemical storage system, *Appl. Therm. Eng.* 120 (2017) 626–634.
- C. Xu, Z. Yu, Y. Xie, Y. Ren, F. Ye, X. Ju, Study of the hydration behavior of zeolite-MgSO₄ composites for long-term heat storage, *Appl. Therm. Eng.* 129 (2018) 250–259.
- T. Yan, R.Z. Wang, T.X. Li, L.W. Wang, I.T. Fred, A review of promising candidate reactions for chemical heat storage, *Renew. Sustain. Energy Rev.* 43 (2015) 13–31.
- A. Solé, I. Martorell, L.F. Cabeza, State of the art on gas–solid thermochemical energy storage systems and reactors for building applications, *Renew. Sustain. Energy Rev.* 47 (2015) 386–398.
- W. Li, J.J. Klemes, Q. Wang, M. Zeng, Development and characteristics analysis of salt-hydrate based composite sorbent for low-grade thermochemical energy storage, *Renew. Energy* 157 (2020) 920–940.
- M. Kubota, S. Matsumoto, H. Matsuda, Enhancement of hydration rate of LiOH by combining with mesoporous carbon for Low-temperature chemical heat storage, *Appl. Therm. Eng.* 150 (2019) 858–863.
- M. Kubota, S. Matsumoto, H. Matsuda, H.Y. Huang, Z.H. He, X.X. Yang, Chemical heat storage with LiOH/LiOH-H₂O reaction for low-temperature heat below 373 K, *Adv. Mater. Res.* (2014) 757–760, 953–954.

- [27] W. Li, J.J. Klemeš, Q. Wang, M. Zeng, Energy storage of low potential heat using lithium hydroxide based sorbent for domestic heat supply, *J. Clean. Prod.* 285 (2021), 124907.
- [28] R. Wang, D. Jin, Y. Zhang, S. Wang, J. Lang, X. Yan, L. Zhang, Engineering metal organic framework derived 3D nanostructures for high performance hybrid supercapacitors, *J. Mater. Chem. 5* (2017) 292–302.
- [29] S. Li, H. Huang, X. Yang, Y. Bai, J. Li, N. Kobayashi, M. Kubota, Hydrophilic substance assisted low temperature LiOH-H₂O based composite thermochemical materials for thermal energy storage, *Appl. Therm. Eng.* 128 (2018) 706–711.
- [30] H.-x. Zhong, J. Wang, Y.-w. Zhang, W.-l. Xu, W. Xing, D. Xu, Y.-f. Zhang, X.-b. Zhang, ZIF-8 derived graphene-based nitrogen-doped porous carbon sheets as highly efficient and durable oxygen reduction electrocatalysts, *Angew. Chem. Int. Ed.* 53 (2014) 14235–14239.
- [31] Z. Li, H.C. Zeng, Surface and bulk integrations of single-layered Au or Ag nanoparticles onto designated crystal planes {110} or {100} of ZIF-8, *Chem. Mater.* 25 (2013) 1761–1768.
- [32] W. Ren, R. Saito, L. Gao, F. Zheng, Z. Wu, B. Liu, M. Furukawa, J. Zhao, Z. Chen, H.-M. Cheng, Edge phonon state of mono- and few-layer graphene nanoribbons observed by surface and interference co-enhanced Raman spectroscopy, *Phys. Rev. B* 81 (2010), 035412.
- [33] X. Yang, S. Li, H. Huang, J. Li, N. Kobayashi, M. Kubota, Effect of carbon nanoadditives on lithium hydroxide monohydrate-based composite materials for low temperature chemical heat storage, *Energies* 10 (2017) 644.
- [34] K. Morishige, Adsorption hysteresis in ordered mesoporous silicas, *Adsorption* 14 (2008) 157–163.
- [35] S. Li, H. Huang, J. Li, N. Kobayashi, Y. Osaka, Z. He, H. Yuan, The effect of 3D carbon nanoadditives on lithium hydroxide monohydrate based composite materials for highly efficient low temperature thermochemical heat storage, *RSC Adv.* 8 (2018) 8199–8208.
- [36] Q. Wang, Y. Xie, B. Ding, G. Yu, F. Ye, C. Xu, Structure and hydration state characterizations of MgSO₄-zeolite 13x composite materials for long-term thermochemical heat storage, *Sol. Energy Mater. Sol. Cell.* 200 (2019), 110047.
- [37] Y.-T. Li, M.-T. Li, Z.-B. Xu, Z.-H. Meng, Q.-P. Wu, Dehydration kinetics and thermodynamics of ZrO(NO₃)₂-doped Ca(OH)₂ for chemical heat storage, *Chem. Eng. J.* 399 (2020), 125841.
- [38] S. Li, H. Huang, X. Yang, C. Wang, N. Kobayashi, M. Kubota, A facile method to construct graphene oxide-based magnesium hydroxide for chemical heat storage, *Nanoscale Microscale Thermophys. Eng.* 21 (2017) 1–7.
- [39] J. Zhu, C. Gao, F. Kong, K. Zhang, Z. Bai, J. Guo, Low-priced stable SrCl₂@SG composite sorbents for low-grade solar heat storage application in open sorption systems, *Sol. Energy Mater. Sol. Cell.* 229 (2021), 111118.
- [40] Y.J. Zhao, R.Z. Wang, Y.N. Zhang, N. Yu, Development of SrBr₂ composite sorbents for a sorption thermal energy storage system to store low-temperature heat, *Energy* 115 (2016) 129–139.
- [41] E. Courbon, P. D'Ans, O. Skrylnyk, M. Frère, New prominent lithium bromide-based composites for thermal energy storage, *Journal of Energy Storage* 32 (2020), 101699.